7-2011

Solvent-Induced Shift of the Lowest Singlet $\pi \rightarrow \pi^*$ Charge-Transfer Excited State of p-Nitroaniline in Water: An Application of the TDDFT/EFP1 Method

Sarom Sok
Iowa State University, ssok1@iastate.edu

Soohaeng Y. Willow
Pohang University of Science and Technology

Federico Zahariev
Iowa State University, fzahari@iastate.edu

Mark S. Gordon
Iowa State University, mgordon@iastate.edu

Solvent-Induced Shift of the Lowest Singlet $\pi \rightarrow \pi^*$ Charge-Transfer Excited State of p-Nitroaniline in Water: An Application of the TDDFT/EFP1 Method

Abstract
The combined time-dependent density functional theory effective fragment potential method (TDDFT/EFP1) is applied to a study of the solvent-induced shift of the lowest singlet $\pi \rightarrow \pi^*$ charge-transfer excited state of *p*-nitroaniline (*p*NA) from the gas to the condensed phase in water. Molecular dynamics simulations of *p*NA with 150 EFP1 water molecules are used to model the condensed-phase and generate a simulated spectrum of the lowest singlet charge-transfer excitation. The TDDFT/EFP1 method successfully reproduces the experimental condensed-phase $\pi \rightarrow \pi^*$ vertical excitation energy and solvent-induced red shift of *p*NA in water. The largest contribution to the red shift comes from Coulomb interactions, between*p*NA and water, and solute relaxation. The solvent shift contributions reflect the increase in zwitterionic character of *p*NA upon solvation.

Disciplines
Chemistry

Comments
Reprinted (adapted) with permission from *Journal of Physical Chemistry A* 115 (2011): 9801, doi:10.1021/jp2045564.

THE JOURNAL OF PHYSICAL CHEMISTRY A

ARTICLE

pubs.acs.org/JPCA

Solvent-Induced Shift of the Lowest Singlet $\pi \rightarrow \pi^*$ Charge-Transfer Excited State of *p*-Nitroaniline in Water: An Application of the TDDFT/EFP1 Method

Sarom Sok,[†] Soohaeng Y. Willow,[‡] Federico Zahariev,[†] and Mark S. Gordon*[,†]

[†]Department of Chemistry and Ames Laboratory, Iowa State University, Ames, Iowa 50011-3111, United States

[‡]Center for Superfunctional Materials, Department of Chemistry, Pohang University of Science and Technology, San 31, Hyojadong, Namgu, Pohang 790-784, Korea

Supporting Information

ABSTRACT: The combined time-dependent density functional theory effective fragment potential method (TDDFT/EFP1) is applied to a study of the solvent-induced shift of the lowest singlet $\pi \rightarrow \pi^*$ charge-transfer excited state of *p*-nitroaniline (*p*NA) from the gas to the condensed phase in water. Molecular dynamics simulations of *p*NA with 150 EFP1 water molecules are used to model the condensed-phase and generate a simulated spectrum of the lowest singlet charge-transfer excitation. The TDDFT/EFP1 method successfully reproduces the experimental condensed-phase $\pi \rightarrow \pi^*$ vertical excitation energy and solvent-induced red shift of *p*NA in water. The largest contribution to the red shift comes from Coulomb interactions, between *p*NA and water, and solute relaxation. The solvent shift contributions reflect the increase in zwitterionic character of *p*NA upon solvation.

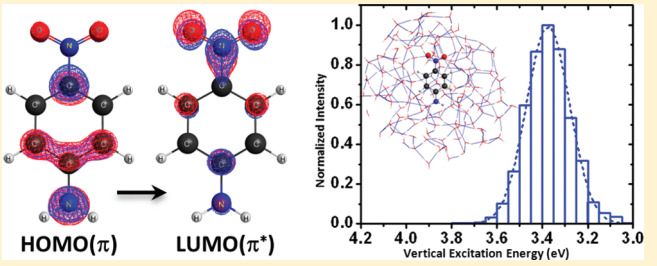

1. INTRODUCTION

The ability to interpret, guide, and model experiments is one of the major goals of quantum chemistry. Several computational methods are available to calculate the electronic properties of small- and medium-sized gas phase molecules in the excited state. Examples include time-dependent density functional theory (TDDFT), singly excited configuration interaction with perturbative doubles (CIS(D)), equation-of-motion coupled cluster with single and double excitations (EOM-CCSD), and multireference (MR) methods such as MR configuration interaction and MR perturbation theory.[1] However, most experiments occur in solution, and the effect of the surrounding environment (solvent) needs to be taken into account in order to accurately describe a molecular system in the condensed phase.[2,3]

The approaches for modeling environmental effects can be divided into three categories:

1. "Supermolecular solvation" models environmental effects by explicitly including the solvent molecules and treating the entire system with the same level of quantum mechanics (QM). The treatment of long-range solvent effects and the applicability to extended systems are limited because the computational scaling of supermolecular QM methods is dependent on the level of theory employed; e.g., N^4 scaling for TDDFT, N^5 scaling for CIS(D), and N^6 scaling for EOM-CCSD where N is a measure of the system size.[4]
2. "Continuum solvation" places the solute in a molecular cavity and replaces the solvent with a homogeneous medium represented by a dielectric constant. Continuum methods are computationally efficient, reasonably accurate for bulk properties, and able to treat large molecules.[5] However, the weaknesses of the continuum solvation approach are the sensitivity to cavitation properties[6,7] and the inability to treat specific solute−solvent interactions, such as hydrogen bonding,[8,9] due to the lack of explicit solvent molecules.
3. "Discrete solvation" treats each component of the environment explicitly and specific solute−solvent interactions are taken into account. The computational complexity and accuracy of discrete methods are dependent on the level of sophistication and empiricism of the potentials used. Bulk characteristics of the solvent are frequently obtained using molecular dynamics or Monte Carlo simulations through a hybrid quantum mechanics/molecular mechanics (QM/MM) approach.[10−14] Sufficient sampling of configurations becomes a bottleneck with QM/MM methods as the size of the environment increases,[15] thereby driving the need for accurate and computationally efficient discrete solvation approaches.

Of the three different solvation approaches, the discrete method offers an appealing compromise between accuracy and

Received: May 16, 2011
Revised: July 27, 2011
Published: July 28, 2011

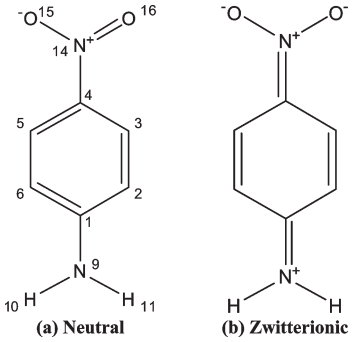

Figure 1. Neutral and zwitterionic resonance structures of *p*-nitroaniline.

computational scalability, especially when the solvent−solute interactions include hydrogen bonding.

The effective fragment potential (EFP) method is a discrete QM-based approach for modeling environmental effects.[16−20] The original EFP method, EFP1, was developed to describe the condensed-phase of water and has been successfully applied to the study of water clusters,[21−24] chemical reactions in aqueous solution,[25,26] environmental effects on biomolecular systems,[27−30] and solvent effects on electronic excitations.[31−35] The EFP1 method consists of three terms that represent the important intermolecular (nonbonded) interactions that are added as one-electron contributions to the quantum mechanical Hamiltonian of the solute: Coulomb (electrostatic), induction (polarization), and a remainder term to account for all interactions not captured by the first two terms. In the Hartree−Fock (HF) based EFP1 method, the remainder term contains exchange repulsion and charge transfer.[16] In the density functional theory (DFT) based EFP1 method, the remainder term also includes short-range electron correlation.[17] In EFP1, the remainder term is fitted to two separate functional forms depending on whether one is considering solute−solvent or solvent−solvent interactions. Because the EFP1 solute−solvent interaction potentials consist of only one-electron integrals, the computational overhead for including environmental effects is small compared to the QM method used. The EFP1 method for water has been interfaced with HF,[16] DFT,[17,19] multiconfigurational self-consistent field (MCSCF),[26] singly excited configuration interaction (CIS),[31] EOM-CCSD,[32] and CIS(D).[33] Recently, the EFP1 method has been interfaced with TDDFT for excited states, permitting the study of optical properties of chromophores in aqueous media.[34,35]

p-Nitroaniline (*p*NA), Figure 1, is an important prototypical organic push−pull (donor-π-acceptor) chromophore and has been the subject of many theoretical[32,33,36−46] and experimental[47−54] studies. *p*NA can be represented by two mesomeric structures: neutral and zwitterionic.[47] Changes within the conjugated molecular framework of the neutral form (Figure 1a), through transfer of charge or distortions caused by solvent interactions, can increase the importance of the zwitterionic form (Figure 1b). The degree of zwitterionic character reflects the amount of charge separation. For donor-π-acceptor molecules, the increase in zwitterionic character and the subsequent increase in dipole moment are stabilized in polar solvents through solvent interactions such as hydrogen bonding.[2] *p*NA possesses a strong $\pi \rightarrow \pi^*$ absorption band in the near-ultraviolet to visible spectral region.[36] The low lying singlet excited state is associated with an intramolecular charge transfer from the amino group to the nitro group across the phenyl ring, leading to a change in the dipole moment of *p*NA.[37,38] The peak of the $\pi \rightarrow \pi^*$ absorption band is strongly dependent on the solvent polarity due to the increase in the dipole moment upon photoexcitation.[39,48] Twisting of the nitro group relative to the conjugated framework lowers the energy of the charge-transfer excited state and increases the dipole moment.[37−50] An experimental −0.98 eV red shift of the charge-transfer excited state is observed upon going from the gas phase, 4.24 eV,[48] to the aqueous phase, 3.26 eV.[49,50]

Recently, Slipchenko used the EFP method for water and EOM-CCSD for *p*NA to investigate the solvent-induced shift of the singlet $\pi \rightarrow \pi^*$ charge-transfer excited state of *p*NA−water$_n$ complexes (n = 2, 4, 6).[32] Slipchenko observed that the polarization response of the solvent to the excited state electron density contributes less than ≈5% to the total solvent-induced red shift. The largest contributions to the solvent shift come from "indirect" contributions, where "indirect" contributions refer to the orbital relaxation of the ground state of the solute in the presence of the electrostatic field of the solvent. The largest "indirect" contribution to the solvent shift, about 80%, is from the Coulomb interactions between *p*NA and water.

In a related study, Kosenkov and Slipchenko investigated the solvent-induced shift of *p*NA in water using a QM/MM (CIS(D)/EFP) approach.[33] Molecular dynamics (MD) simulations of *p*NA and 64 EFP solvent molecules using periodic boundary conditions, in which the *p*NA geometry was frozen, were used to model the condensed phase. These calculations reproduced the red shift of the lowest singlet $\pi \rightarrow \pi^*$ charge-transfer excited state in water to within 0.02 eV of experiment and the spectral line width in the condensed phase to within 0.14 eV of experiment. However, the experimental gas and condensed phase vertical excitation energies for the singlet charge transfer state were overestimated by 0.41 and 0.39 eV, respectively.

In the current work, the TDDFT/EFP1 method is used to study the lowest singlet $\pi \rightarrow \pi^*$ charge-transfer excited state of *p*NA in water. MD simulations of *p*NA with 150 EFP1 water molecules are used to model the condensed phase. The solvent-induced (solvatochromic) shift from the gas to the condensed phase is calculated and compared with experiment. The density functional dependence of the calculated solvent shifts is investigated, and the accuracy and computational efficiency of the TDDFT/EFP1 method is discussed.

The structure of this paper is as follows. The next section briefly describes the TDDFT/EFP1 method. This is followed by a summary of the computational details, the results, and a discussion of the calculations. Concluding remarks are given in the last section.

2. THE TD-DFT/EFP1 METHOD

The formulation of the TDDFT/EFP1 method has been described by Yoo et al.[34] and Minezawa et al.;[35] therefore, the method is only briefly summarized here. In the TDDFT/EFP1 method the solvent is treated with EFP1/DFT[16,17,19] and the interaction energy is a sum of three terms

$$E_{\text{Interaction}}^{\text{EFP1}} = \sum_{\eta}\left[\sum_{k=1}^{K} E_k^{\text{Coul}}(\eta) + \sum_{l=1}^{L} E_l^{\text{pol}}(\eta) + \sum_{m=1}^{M} E_m^{\text{rem}}(\eta)\right] \quad (1)$$

where η sums over the solvent molecules. For the ηth solvent molecule, these contributions are expanded over a number (K, L, and M) of expansion points.

The first term in eq 1 represents the Coulomb interaction and is expressed using a distributed multipolar expansion of the fragment molecular density, carried out through octopole moments. For water, $K = 5$ expansion points are used (atom centers and bond midpoints). The Coulomb term is scaled by a distance-dependent damping term to account for overlapping charge densities at small intermolecular distances.

The second term in eq 1 represents the polarization interaction energy and is represented using localized molecular orbital (LMO) polarizability tensors. For water, $L = 5$ expansion points are used, centered at the two O−H bonds and the two oxygen lone pairs. The polarization term is iterated within the Kohn−Sham iterations until self-consistency is reached.

The last term in eq 1 is a remainder term containing interaction energy components not captured by the Coulomb and polarization terms. The remainder term is fitted to a functional form by first computing the water dimer potential energy and then subtracting the first two terms in eq 1 from the quantum mechanical (QM) water dimer potential. If a HF based water dimer potential is used, the remainder term will contain the exchange repulsion and charge transfer interaction energies. If a DFT based water dimer potential is used, the remainder term will also include some short-range electron correlation.

The EFP1 water molecules are allowed to rotate and translate, but the internal geometry is fixed. The bond length and bond angle of an EFP1/DFT water molecule are 0.9468 Å and 106.70°, respectively.

In the TDDFT/EFP1 method, the linear response formulation of the TDDFT equations is used[55−59]

$$\begin{bmatrix} \mathbf{A} & \mathbf{B} \\ \mathbf{B} & \mathbf{A} \end{bmatrix} \begin{bmatrix} \mathbf{X} \\ \mathbf{Y} \end{bmatrix} = \omega \begin{bmatrix} 1 & 0 \\ 0 & -1 \end{bmatrix} \begin{bmatrix} \mathbf{X} \\ \mathbf{Y} \end{bmatrix} \tag{2}$$

Solutions to the non-Hermitian eigenvalue problem in eq 2 yield the transition energy, ω, and the corresponding biorthonormal transition vectors $\mathbf{X}$ and $\mathbf{Y}$. The matrices $\mathbf{A}$ and $\mathbf{B}$ in eq 2 are defined as

$$A_{ia\mu,jb\nu} = \delta_{ij}\delta_{ab}\delta_{\mu\nu}(\varepsilon_a - \varepsilon_i) + K_{ia\mu,jb\nu} \tag{3}$$

and

$$B_{ia\mu,jb\nu} = K_{ia\mu,bj\nu} \tag{4}$$

where indices i, j and a, b label occupied and virtual orbitals, respectively, while the indices μ, ν denote spin. ε_a and ε_i are orbital energies for Kohn−Sham orbitals ϕ_a and ϕ_i, respectively. The coupling matrix[60] $K_{ia\mu,jb\nu}$ is given by

$$K_{ia\mu,jb\nu} = \iint \phi^*_{i\mu}(\mathbf{r})\phi_{a\mu}(\mathbf{r})\left(\frac{1}{|\mathbf{r}-\mathbf{r}'|} + \frac{\delta^2 E_{xc}}{\delta\rho_\mu(\mathbf{r})\delta\rho_\nu(\mathbf{r}')}\right)\phi_{j\nu}(\mathbf{r}')\phi^*_{b\nu}(\mathbf{r}')\,d\mathbf{r}\,d\mathbf{r}' \tag{5}$$

where E_{xc} is the exchange-correlation energy. ρ_μ and ρ_ν are electron spin densities.

The only EFP1 term that contributes to the coupling matrix $\mathbf{K}$, after taking the second functional derivative with respect to the electron density, is the polarization, so that the EFP1-modified coupling matrix $\mathbf{K}$ becomes

$$\begin{aligned} K_{ia\mu,jb\nu} = {} & \iint \phi^*_{i\mu}(\mathbf{r})\phi_{a\mu}(\mathbf{r})\left(\frac{1}{|\mathbf{r}-\mathbf{r}'|}\right)\phi_{j\nu}(\mathbf{r}')\phi^*_{b\nu}(\mathbf{r}')\,d\mathbf{r}\,d\mathbf{r}' \\ & + \iint \phi^*_{i\mu}(\mathbf{r})\phi_{a\mu}(\mathbf{r})\left(\frac{\delta^2 E_{xc}}{\delta\rho_\mu(\mathbf{r})\delta\rho_\nu(\mathbf{r}')}\right)\phi_{j\nu}(\mathbf{r}')\phi^*_{b\nu}(\mathbf{r}')\,d\mathbf{r}\,d\mathbf{r}' \\ & + \iint \phi^*_{i\mu}(\mathbf{r})\phi_{a\mu}(\mathbf{r})\left(\frac{\delta^2 E^{pol}}{\delta\rho_\mu(\mathbf{r})\delta\rho_\nu(\mathbf{r}')}\right)\phi_{j\nu}(\mathbf{r}')\phi^*_{b\nu}(\mathbf{r}')\,d\mathbf{r}\,d\mathbf{r}' \end{aligned} \tag{6}$$

The EFP1 solvent molecules affect the TDDFT excited state calculation directly through the polarization term in the modified coupling matrix $\mathbf{K}$ and indirectly through changes in the solute geometry (solute relaxation) and ground state electron density due to the presence of the effective fragments. Previous works[31,35,83] have shown that consideration of the excited state electron density with respect to the response of the solvent polarization makes a very small contribution to the calculated excitation energies; therefore, it is not taken into account in the current study.

3. COMPUTATIONAL DETAILS

Solvatochromic shift values are calculated as the differences between the gas and condensed phase vertical excitation energies of the solute. The statistically averaged condensed phase vertical excitation energy is obtained in a two-step process. First, a molecular dynamics simulation is used to obtain a set of representative configurations (~2000 snapshots) of the solute−solvent system. Then the lowest singlet $\pi \rightarrow \pi^*$ TDDFT vertical excitation energy is calculated for each configuration. The condensed phase vertical excitation energy of the solute is taken as the central value of a Gaussian function fitted to the histogram of calculated vertical excitation energies.

Molecular Dynamics Simulation. A Born−Oppenheimer ab initio MD simulation was performed on a nonperiodic system consisting of *p*NA surrounded by 150 water molecules, within the canonical ensemble (NVT) at a fixed temperature of 300 K using a Nosé-Hoover thermostat.[61] The 150 water molecules (MM region) were treated as DFT-based EFP1 fragments, called EFP1/DFT.[17,19] The *p*NA molecule (QM region) was treated with DFT using the Becke three-parameter (exchange)[62] and Lee−Yang−Parr (correlation)[63] (B3LYP) hybrid functional[64] and the Dunning−Hay basis set[65] with d polarization functions on oxygen and p polarization functions on hydrogen atoms (DH(d,p)), to be consistent with the functional and basis set used to develop EFP1/DFT. The isolated system was equilibrated for 20 ps with a 1.0 fs time step. Snapshots were collected every 10 time steps from a 20 ps production run giving a total of 2000 configurations.

Vertical Excitations. Both gas and condensed phase vertical excitation energies were calculated using TDDFT with the B3LYP functional (TD-B3LYP) and the DH(d,p) basis set. The structure of the solute used in the gas phase excited state calculation was obtained from the optimized ground state geometry of *p*NA calculated at the B3LYP/DH(d,p) level of theory, in C_1 symmetry. Structures used in the condensed phase vertical excitation energy calculations were obtained from snapshots of the QM/MM (B3LYP/EFP1) MD simulation production run.

Table 1. Ground State Structural Parameters (in Angstroms and Degrees) Calculated for *p*-Nitroaniline (see Figure 1)

	gas phase			condensed phase
	B3LYP[a]	MP2[b]	exptl[c]	B3LYP-EFP1[d]
$R(C_2-C_1)$	1.416	1.411	1.41	1.434 (0.027)
$R(C_3-C_2)$	1.391	1.394	1.37	1.380 (0.026)
$R(C_4-C_3)$	1.403	1.398	1.39	1.421 (0.028)
$R(C_1-N_9)$	1.355	1.379	1.35	1.346 (0.025)
$R(C_4-N_{14})$	1.461	1.465	1.45	1.412 (0.031)
$R(N_{14}-O_{15})$	1.240	1.247	1.23	1.264 (0.024)
$\theta(C_2C_1N_9H_{10})$	19.9			10.0 (7.4)
$\theta(C_5C_4N_{14}O_{15})$	0.0			7.9 (6.0)

[a] This work. From an optimized gas-phase structure obtained at the B3LYP/DH(d,p) level of theory. [b] Reference 40. [c] Reference 51. [d] From an average of 2000 snapshots of *p*-nitroaniline with 150 EFP1 water molecules during the QM/MM (B3LYP/EFP1) MD simulation. Standard deviations are in parentheses.

Additional TDDFT calculations with the Perdew−Berke−Ernzerhof hybrid[66,67] (TD-PBE0) and the Coulomb-attenuated method B3LYP[68] functional (TD-CAM-B3LYP) and the DH(d,p) basis set were performed to investigate the density functional dependence of the solvatochromic shift. In the TD-PBE0 and TD-CAM-B3LYP calculations, the optimized gas phase structure of *p*NA obtained at the B3LYP/DH(d,p) level of theory and the 2000 condensed phase snapshots of *p*NA with 150 EFP1 water molecules obtained from the QM/MM (B3LYP/EFP1) MD simulation production run were used.

Both ground state DFT and excited state TDDFT calculations were carried out using the (96, 1202) Euler−MacLaurin radial[69] and Lebedev angular[70] grid. For computational efficiency, the MD simulation employed a smaller (96, 590) Euler−MacLaurin radial and Lebedev angular grid.

Lambda Diagnostic. The lambda diagnostic of Peach et al.[71] quantifies the degree of orbital overlap between occupied-virtual pairs (transition vectors) contributing to an excited state. Λ is calculated as the sum of spatial overlaps, O_{ia}, between transition vectors involved in an excited state weighted by the square of the transition amplitude κ_{ia}

$$\Lambda = \frac{\sum_{ia} \kappa_{ia}^2 O_{ia}}{\sum_{ia} \kappa_{ia}^2} \tag{7}$$

where the spatial overlap is given as the inner product of the moduli of occupied and virtual Kohn−Sham orbitals, ϕ_i and ϕ_a

$$O_{ia} = \langle |\phi_i||\phi_a| \rangle = \int |\phi_i(\mathbf{r})||\phi_a(\mathbf{r})|\, d\mathbf{r} \tag{8}$$

and

$$\kappa_{ia} = \mathbf{X}_{ia} + \mathbf{Y}_{ia} \tag{9}$$

X and **Y** are the transition vectors defined in eq 2. Lambda values range from 0 to 1 with small lambda values indicating low-overlap/long-range excitations (e.g., Rydberg excited states) and large lambda values signifying high-overlap/short-range excitations (e.g., low-lying valence excited states). Charge-transfer excited states possess intermediate lambda values. Several studies have demonstrated errors in calculated excitation energies for small lambda values and large charge-transfer character.[71−76] Excitation energies with lambda values <0.3 for hybrid density functionals are most likely to be significantly underestimated. The lambda diagnostic of Peach et al. is used in the current study to assess the degree of charge transfer for the lowest singlet $\pi \rightarrow \pi^*$ intramolecular charge-transfer excited state of *p*NA.

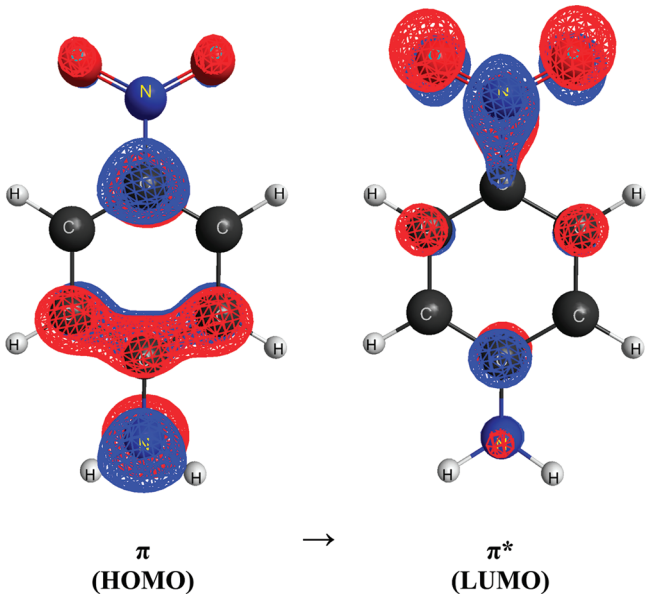

Figure 2. Kohn−Sham molecular orbitals of dominant linear response TD-B3LYP/DH(d,p) transition vector for the lowest singlet $\pi \rightarrow \pi^*$ charge transfer excitation of *p*-nitroaniline in the gas phase.

Partial atomic charges were calculated using the geodesic electrostatic potential derived charge method of Spackman.[77] All calculations were performed using the General Atomic and Molecular Electronic Structure System (GAMESS) quantum chemistry code[78] and visualized using MacMolPlt.[79]

4. RESULTS AND DISCUSSION

Calculations in the Gas Phase. Geometric parameters for the B3LYP/DH(d,p) optimized gas-phase structure of *p*NA are summarized in Table 1. The gas-phase structure of *p*NA in the ground state is nearly planar with a dihedral angle on the amino group of ≈±20°. The predicted bond lengths are in reasonable agreement with the MP2 calculations of Sim et al. using a double-ξ quality basis set[40] and the experimental crystallography data of Trueblood et al.[51] The calculated dipole moment of 7.3 D is comparable to the experimental measurement of Breitung et al.[52] in dilute benzene solution, 7.6 D, and CIS(D) studies of Kosenkov and Slipchenko, 7.7 D.[33]

For the optimized gas phase structure of *p*NA, TD-B3LYP/DH(d,p) predicts a vertical excitation energy of 3.97 eV for the lowest singlet $\pi \rightarrow \pi^*$ transition; a lambda diagnostic value of 0.593 indicates that this transition has charge-transfer character. The calculated gas phase dipole moment of *p*NA is found to increase in the excited state to 12.5 D. The dominant transition vector contributing to the description of the singlet charge-transfer excited state of *p*NA in the gas phase involves excitation from the highest occupied molecular orbital (HOMO) to the lowest unoccupied molecular orbital (LUMO). These orbitals are illustrated in Figure 2. The predicted value for the excitation energy of the singlet charge-transfer excited state is

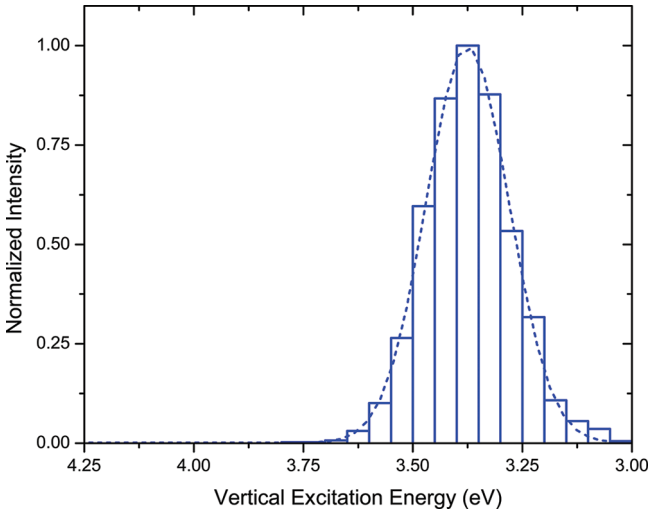

Figure 3. Simulated condensed-phase spectrum for the $\pi \rightarrow \pi^*$ excitation of *p*-nitroaniline (dashed line). Gaussian function centered at 3.37 eV fitted to the histogram of calculated $\pi \rightarrow \pi^*$ vertical excitation energies from QM/MM (B3LYP/EFP1) MD simulation.

underestimated by 0.27 eV, compared to the experimental gas-phase value of 4.24 eV.[48] The CIS(D) calculations of Kosenkov and Slipchenko overestimate the gas phase charge-transfer excitation energy of *p*NA by 0.41 eV.[33] Kosenkov and Slipchenko attribute the discrepancy in the calculated gas phase value to the use of a small basis set. Improvement in the TDDFT calculated vertical excitation energy can be achieved by increasing the basis set, as shown by Scalmani et al.[41] using the 6-311G(d,p) basis set and the B3LYP functional, 4.07 eV, or using a density functional designed to have a proper long-range (asymptotic) behavior of the exchange-correlation potential.

Calculations in Aqueous Solution. MD simulations of *p*NA with 150 EFP1 water molecules were performed to model the condensed phase. During an MD simulation, the solute geometry and hydrogen-bonding arrangement of the solvent cage is allowed to fluctuate, producing a distribution of configurations. A representative structure is illustrated in Figure 1S (see Supporting Information). Averaged values are reported for all condensed phase properties calculated.

The averaged geometric parameters for the condensed phase structure of *p*NA in the ground state are summarized in Table 1. Structural changes of *p*NA upon solvation are marked by a modest increase in the nitro $N_{14}-O_{15}$ bond and a small shortening of the phenyl C_2-C_3 and nitro C_4-N_{14} bond. The change in bond lengths is accompanied by a decrease in the dihedral angles of the amino and nitro groups of $\approx\pm 10°$ and $\approx\pm 7°$, respectively. The calculated ground state dipole moment of *p*NA in the aqueous phase is 16.2 D. The significant increase in the dipole moment of *p*NA in the condensed phase is in qualitative agreement with the semiempirical calculations of Farztdinov et al.[39] and of Kovalenko et al.[50] Table 1S in the Supporting Information presents B3LYP/DH(d,p) calculated gas and condensed phase partial atomic charges on the nitrogens in the amino and nitro groups of *p*NA, exhibiting an increase in negative and positive charge, respectively. This reflects an increase in the charge separation upon solvation. The observed structural changes, increase in dipole moment, and charge separation are indicative of an increase in the zwitterionic character of the ground-state structure of *p*NA in the condensed phase.

Table 2. Calculated and Experimental Solvent-Induced Shifts (in eV) for the $\pi \rightarrow \pi^*$ Charge-Transfer Excited State of *p*-Nitroaniline

$\pi \rightarrow \pi^*$	experimental	calculated
gas phase	4.24[a]	3.97[c]
condensed phase	3.26[b]	3.37[d]
shift	−0.98	−0.60

[a] Reference 48. [b] References 49 and 50. [c] From an optimized B3LYP/DH(d,p) gas phase structure. [d] From an average of 2000 snapshots of *p*-nitroaniline with 150 EFP1 water molecules during the QM/MM (B3LYP/EFP1) MD simulation.

The simulated spectrum of the lowest singlet $\pi \rightarrow \pi^*$ charge-transfer excited state of *p*NA in the condensed phase is shown in Figure 3. The TD-B3LYP/EFP1 calculated charge-transfer band is centered at 3.37 eV with a lambda diagnostic value of 0.677. The calculated excited state dipole moment of *p*NA in the condensed phase is 17.0 D. The predicted value for the singlet $\pi \rightarrow \pi^*$ excitation is in good agreement (within 0.11 eV) with the experimental value of 3.26 eV.[49,50] However, the TD-B3LYP/EFP1 predicted spectral full line width at half-maximum (fwhm), 0.23 eV, underestimates the experimental value of 0.6 eV.[50] Predicting spectral line widths that are in agreement with experiment may require the use of periodic boundary conditions, as was done by Kosenkov and Slipchenko.[33]

Solvent Shift. Table 2 compares the calculated and experimental solvent-induced shifts for the lowest singlet $\pi \rightarrow \pi^*$ charge-transfer excited state of *p*NA. Going from the gas to the condensed phase, TD-B3LYP/EFP1 predicts a red shift for the lowest singlet $\pi \rightarrow \pi^*$ excitation energy in agreement with previous theoretical[33,39] and experimental[49,50] observations. The magnitude of the calculated solvent shift, −0.60 eV, is underestimated by 0.38 eV compared to the experimental value of −0.98 eV.

Approximately 70% of the error in the predicted solvent shift is due to the underestimation of the calculated gas phase value of the $\pi \rightarrow \pi^*$ excitation energy. The error in the gas phase value is likely to be due to the charge-transfer nature of the lowest singlet $\pi \rightarrow \pi^*$ excited state of *p*NA and the incorrect long-range behavior of the exchange functional used in the TDDFT calculation.[80−82] Intramolecular charge-transfer excitations using the B3LYP functional possess intermediate lambda values for *p*NA in the gas phase, 0.593 for the lowest singlet $\pi \rightarrow \pi^*$ charge-transfer excited state. In the condensed phase, the lambda value increases to 0.677. Improvement in the description of charge-transfer excited states in both the gas and condensed phase may be achieved by using or increasing the amount of nonlocal exchange as suggested in the literature.[80]

Table 3 summarizes the density functional dependence of the calculated solvent shift. The CIS(D) calculated solvent-induced shift of Kosenkov and Slipchenko[33] is provided in Table 3 for comparison. The quality of the calculated solvent shift improves slightly upon going from TD-B3LYP to TD-PBE and more significantly when TD-CAM-B3LYP is employed. The improvement mirrors the amount of nonlocal (HF) exchange used in the description of the density functionals. The amount of HF exchange in B3LYP, PBE0, and CAM-B3LYP is 20%, 25%, and 19−65%, respectively. The range for CAM-B3LYP arises

Table 3. Comparison of Calculated Solvent-Induced Shifts (in eV) for the $\pi \rightarrow \pi^*$ Charge-Transfer Excited State of *p*-Nitroaniline in Water

	calculated			
$\pi \rightarrow \pi^*$	TD-B3LYP/DH(d,p)	TD-PBE0/DH(d,p)	TD-CAM-B3LYP/DH(d,p)	CIS(D)[g]
gas phase	3.97[a]	4.11[c]	4.40[e]	4.65
condensed phase	3.37[b]	3.44[d]	3.50[f]	3.65
shift (condensed − gas)	−0.60	−0.67	−0.90	−1.00

[a] From an optimized gas phase structure obtained at the B3LYP/DH(d,p) level of theory. [b] From an average of 2000 snapshots of *p*-nitroaniline with 150 EFP1 water molecules during the QM/MM (B3LYP/EFP1) MD simulation. [c] From TD-PBE0/DH(d,p) calculation on an optimized gas phase structure obtained at the B3LYP/DH(d,p) level of theory. [d] From an average of TD-PBE0-EFP1/DH(d,p) calculations performed on 2000 snapshots of *p*-nitroaniline with 150 EFP1 water molecules during the QM/MM (B3LYP/EFP1) MD simulation. [e] From TD-CAM-B3LYP/DH(d,p) calculation on an optimized gas phase structure obtained at the B3LYP/DH(d,p) level of theory. [f] From an average of TD-CAM-B3LYP-EFP1/DH(d,p) calculations performed on 2000 snapshots of *p*-nitroaniline with 150 EFP1 water molecules during the QM/MM (B3LYP/EFP1) MD simulation. [g] Reference 33.

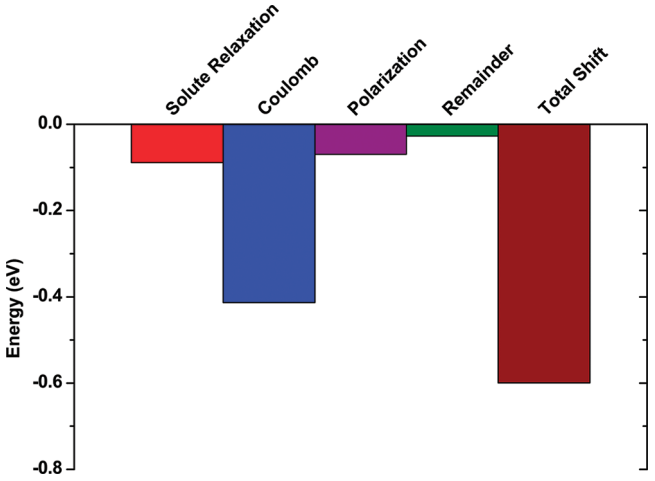

Figure 4. Contributions to the TD-B3LYP-EFP1/DH(d,p) solvent-induced shift of *p*-nitroaniline. Each energy term is obtained from an average of 2000 snapshots of *p*-nitroaniline with 150 EFP1 water molecules during the QM/MM (B3LYP/EFP1) MD simulation.

Table 4. Calculated Dipole Moments (in Debye) of *p*-Nitroaniline[a]

	ground state	excited state
gas phase[b]	7.6	12.5
condensed phase[c]	16.2	17.0

[a] Excited state values correspond to the lowest singlet $\pi \rightarrow \pi^*$ charge transfer state. [b] From an optimized gas phase structure obtained at the B3LYP/DH(d,p) level of theory. [c] From an average of 2000 snapshots of p-nitroaniline with 150 EFP1 water molecules during the QM/MM (B3LYP/EFP1) MD simulation.

Table 5. Contributions (eV) to the Calculated Solvent-Induced Shift of the Lowest Singlet $\pi \rightarrow \pi^*$ Charge-Transfer Excited State of *p*-Nitroaniline in Water[a]

contribution	TD-B3LYP/DH(d,p)	TD-PBE0/DH(d,p)	TD-CAM-B3LYP/DH(d,p)
solute relaxation	−0.09	−0.12	−0.22
Coulomb	−0.41	−0.42	−0.39
polarization	−0.07	−0.10	−0.26
remainder	−0.03	−0.03	−0.03
total shift	−0.60	−0.67	−0.90

[a] Each energy term is obtained from an average of 2000 snapshots of *p*-nitroaniline with 150 EFP1 water molecules during the QM/MM (B3LYP/EFP1) MD simulation.

because this exchange functional is divided into a short-range (19% HF exchange) and a long-range (65% HF exchange) term. The flexibility in the treatment of short-range and long-range effects improves the TD-CAM-B3LYP description of charge-transfer and Rydberg excited states. The TD-CAM-B3LYP solvent shift, −0.90 eV, is in good agreement with the experimental solvent shift, −0.98 eV, and the CIS(D) calculated solvent shift, −1.00 eV, predicted by Kosenkov and Slipchenko.[33]

Contributions to the Solvent Shift. Solvatochromic shifts of vertical excitation energies may be caused by changes in the solute geometry due to solvation (solute relaxation) and specific solute−solvent interactions. In order to understand the contributions of the solute relaxation and solute−solvent interactions to the calculated solvent shift, the QM-EFP intermolecular interaction energy analysis of DeFusco et al.[83] is used to partition the predicted solvent shift into four terms: solute relaxation, Coulomb, polarization, and remainder. The solute relaxation energy is defined as the contribution to the solvent shift from the changes in the solute geometry as a result of solvation. The Coulomb, polarization, and remainder terms correspond to the QM-EFP intermolecular interactions that are summarized in eq 1.

The energy decomposition for the TD-B3LYP/EFP1 calculated solvent-induced shift of the lowest singlet $\pi \rightarrow \pi^*$ charge-transfer excited state of *p*NA is illustrated in Figure 4. The largest contribution to the calculated red shift, ≈ 65% (−0.41 eV), comes from the Coulomb interactions between *p*NA and water. To explore the source of the large electrostatic contribution to the solvent-induced shift, consider the dipole moments summarized in Table 4. The Coulomb contribution can be interpreted in terms of the increase in dipole moment of *p*NA going from the gas phase to the condensed phase. This dipole moment increase is about twice as large in the ground state (∼8.6 D) as in the excited state (∼4.5 D). This difference arises because the large zwitterionic charge separation in the excited state is ameliorated somewhat by the polar solvent.[2,84] In water, the stabilization of the increased dipole moment of *p*NA is likely achieved through hydrogen bonding. Indeed, on average, *p*NA is hydrogen bonded to three EFP1 water molecules. The second largest contribution to the calculated red shift, −0.09 eV ≈ 15%, is due to solute relaxation, reflecting the increase in zwitterionic

Table 6. Comparison of Supermolecular TD-B3LYP/DH(d,p) and TD-B3LYP-EFP1/DH(d,p) Values for a Single QM/MM (B3LYP/EFP1) MD Snapshot of *p*-Nitroaniline with 150 Waters[a]

single MD snapshot (Figure 1S, Supporting Information)	TD-B3LYP/DH(d,p) (150 DFT waters)	TD-B3LYP-EFP1/DH(d,p) (150 EFP1 waters)
$\pi \rightarrow \pi^*$ vertical excitation energy (eV)	3.33	3.49
total wall clock time (no. of CPUs/no. of nodes)	25783.6 min (4/4)	7.6 min (4/4)
replicated memory	19.8 GB	57.9 MB

[a] Calculations performed on a cluster consisting of dual 2.93 GHz quad core X5570 (Nehalem) nodes with 24 GB of memory per node interconnected by an Infiniband QDR (8 Gbit/s) network.

character of the solvated geometry inferred from the calculated structural changes and partial atomic charges of *p*NA, listed in Table 1 and in Table 1S in the Supporting Information, respectively. The sum of the solute−solvent polarization interactions and remainder terms contribute the remaining −0.10 eV of the TD-B3LYP/EFP1 calculated solvent shift.

Table 5 summarizes the functional dependence of the contributions to the calculated solvent shift. Improving the functional results in increases in the solute relaxation and polarization contributions, whereas the Coulomb and remainder term are almost unchanged. Since the CAM-B3LYP functional is in excellent agreement with the experimental solvent shift, it is likely that one source of the poorer agreement between B3LYP and experiment is the inability of this functional to correctly capture the solute relaxation and polarization effects. The largest contribution to the calculated solvent shift is still from the Coulomb interaction between *p*NA and water, but these other two contributions are now comparable in magnitude. The increase in the solute relaxation and polarization is likely due to an improved description of the singlet charge-transfer excited state. Similar findings have been reported by Aidas et al., in their study of the $\pi \rightarrow \pi^*$ solvent shift of acrolein in water.[85]

Performance of the TDDFT/EFP1Method. To assess the accuracy and computational efficiency of the TD-DFT/EFP1 method, the lowest singlet $\pi \rightarrow \pi^*$ charge-transfer excited state of a single snapshot from the QM/MM (B3LYP/EFP1) MD simulation of *p*NA with 150 EFP1 water molecules was calculated with the TD-B3LYP/EFP1 method and compared to a supermolecular TD-B3LYP calculation with the 150 EFP1 water molecules replaced with DFT waters. The calculations were performed on a Microsoft Windows HPC Server 2008 R1 cluster consisting of dual 2.93 GHz quad core X5570 i7 (Nehalem) processors with 24 GB of memory per node interconnected by an Infiniband QDR, 8 Gbit/s, network. Table 6 summarizes the calculated $\pi \rightarrow \pi^*$ vertical excitation energy, total wall clock time, and replicated memory requirements. The supermolecular TD-B3LYP singlet $\pi \rightarrow \pi^*$ vertical excitation energy for *p*NA with 150 DFT water molecules is 3.33 eV, in good agreement with the TD-B3LYP/EFP1 value of 3.49 eV. Further, the total wall time for the TD-B3LYP/EFP1 calculation, 7.6 min, is 3 orders of magnitude smaller than the total wall time required for the supermolecular TD-B3LYP calculation, 25783.6 min. The computational efficiency of the TD-B3LYP/EFP1 method is further underscored by the replicated memory requirements, 57.9 megabytes for TD-B3LYP/EFP1 compared to 19.8 gigabytes for TD-B3LYP.

5. CONCLUSION

In this study the solvent-induced shift for the lowest singlet $\pi \rightarrow \pi^*$ charge-transfer excited state of *p*NA in water was investigated using the TD-DFT/EFP1 method. The condensed phase was modeled using QM/MM (B3LYP/EFP1) MD simulations with 150 EFP1/DFT water molecules. Upon going from the gas to the condensed phase in water, an increase in the zwitterionic character of the ground state geometry of *p*NA is predicted. The increase in zwitterionic character is reflected in the structural changes in the molecular framework and an increase in the dipole moment and charge separation of *p*NA in water.

The TD-B3LYP/EFP1 method reproduces the experimentally observed red shift in water. The largest contributions to the calculated solvent shift are from solute−solvent electrostatic interactions and solute relaxation reflecting the observed increase in dipole moment and zwitterionic character of *p*NA.

The discrepancy between the calculated and experimental solvent shift is due in part to the error in the calculated gas phase vertical excitation energy for the lowest singlet $\pi \rightarrow \pi^*$ charge-transfer excited state of *p*NA. However, the TD-B3LYP/EFP1 calculated condensed phase vertical excitation energy of the charge-transfer excited state agrees with experiment[48−50] to within ≈0.1 eV. By use of a density functional with an improved description of long-range effects, an improvement in the calculated solvent shift is obtained.

For a single snapshot, the TD-B3LYP/EFP1 method reproduces the supermolecular TD-B3LYP value of the singlet $\pi \rightarrow \pi^*$ charge-transfer excitation energy of *p*NA with 150 water molecules to within ≈0.16 eV with a 3000-fold decrease in the total wall clock time. The TD-DFT/EFP1 method is shown to be an accurate and efficient discrete approach to modeling environmental effects for the study of optical properties of organic chromophores in aqueous media.

■ ASSOCIATED CONTENT

Supporting Information. Ground-state gas- and condensed-phase calculated partial atomic charges (Table 1S) and an example of a single configuration (snapshot) of *p*-nitroaniline with 150 EFP1 water molecules during the QM/MM (B3LYP/EFP1) MD simulation (Figure 1S). This material is available free of charge via the Internet at http://pubs.acs.org.

■ AUTHOR INFORMATION

Corresponding Author

*E-mail: mark@si.msg.chem.iastate.edu.

■ ACKNOWLEDGMENT

This work was supported by a grant from the Air Force Office of Scientific Research and by a grant from the Microsoft Corporation. Supermolecular TD-B3LYP calculations were performed on the Rhiannon cluster located at the Microsoft Enterprise Engineering Center (EEC) in Redmond, WA. The

authors thank Microsoft for computational resources, Dr. Albert DeFusco for many helpful discussions, and Mr. Leo C. DeSesso for invaluable assistance in reviewing and editing the manuscript.

REFERENCES

(1) *Theory and Applications of Computational Chemistry: The First Forty Years*; Dykstra, C. E., Frenking, G., Kim, K. S., Scuseria, G. E., Eds.; Elsevier: Amsterdam, 2005.
(2) Reichardt, C. *Solvents and Solvent Effects in Organic Chemistry*, 3rd ed.; Wiley-VCH: Weinheim, 2003.
(3) *Solvation Effects in Molecules and Biomolecules: Computational Methods and Applications*; Canuto, S., Eds.; Springer: Berlin, 2008.
(4) Chiba, M.; Federov, D. G.; Kitaura, K. The Fragment Molecular Orbital-Based Time-Dependent Density Functional Theory for Excited States in Large Systems. In *The Fragment Molecular Orbital Method: Practical Applications to Large Molecular Systems*; Federov, D. G., Kitaura, K., Eds.; CRC Press: Boca Raton, FL, 2009; pp 91−118.
(5) *Continuum Solvation Models in Chemical Physics: From Theory to Applications*; Mennucci, B., Cammi, R., Eds.; Wiley: Hoboken, NJ, 2007.
(6) Santoro, F.; Barone, V.; Gustavsson, T.; Improta, R. *J. Am. Chem. Soc.* **2006**, *128*, 16312−16322.
(7) Improta, R.; Barone, V. *J. Mol. Struct.: THEOCHEM* **2009**, *914*, 87−93.
(8) Besley, N. A.; Hirst, J. D. *J. Am. Chem. Soc.* **1999**, *121*, 8559−8566.
(9) Tomasi, J.; Mennucci, B.; Cammi, R. *Chem. Rev.* **2005**, *105*, 2999−3093.
(10) Warshell, A.; Levitt, M. *J. Mol. Biol.* **1976**, *103*, 227−249.
(11) Singh, U. C.; Kollman, P. A. *J. Comput. Chem.* **1986**, *7*, 718−730.
(12) Field, M. J.; Bash, P. A.; Karplus, M. *J. Comput. Chem.* **1990**, *11*, 700−733.
(13) Gao, J.; Luque, F. J.; Orozco, M. *J. Chem. Phys.* **1993**, *98*, 2975−2982.
(14) Gao, J. Methods and Applications of Combined Quantum Mechanical and Molecular Mechanical Potentials. In *Reviews in Computational Chemistry*; Lipkowitz, K. B., Boyd, D. B., Eds.; Wiley-VCH: Weinheim, 1995; Vol. 7, pp 119−185.
(15) Coutinho, K.; Rivelino, R.; Georg, H. C.; Canuto, S. The Sequential QM/MM Method and Its Application to Solvent Effects in Electronic and Structural Properties of Solutes. In *Solvation Effects in Molecules and Biomolecules: Computational Methods and Applications*; Cantuo, S., Eds.; Springer: Berlin, 2008, pp 159−189.
(16) Day, P. N.; Jensen, J. H.; Gordon, M. S.; Webb, S. P.; Stevens, W. J.; Krauss, M.; Garmer, D.; Basch, H.; Cohen, D. *J. Chem. Phys.* **1996**, *105*, 1968−1986.
(17) Adamovic, I.; Freitag, M. A.; Gordon, M. S. *J. Chem. Phys.* **2003**, *118*, 6725−6732.
(18) Gordon, M. S.; Freitag, M. A.; Bandyopadhyay, P.; Jensen, J. H.; Kairys, V.; Stevens, W. J. *J. Phys. Chem. A* **2001**, *105*, 293−307.
(19) Adamovic, I.; Gordon, M. S. *J. Phys. Chem. A* **2005**, *109*, 1629−1636.
(20) Gordon, M. S.; Slipchenko, L.; Li, H.; Jensen, J. H. *Annu. Rep. Comput. Chem.* **2007**, *3*, 177−193.
(21) Merrill, G. N.; Gordon, M. S. *J. Phys. Chem. A* **1998**, *102*, 2650−2657.
(22) Day, P. N.; Pachter, R.; Gordon, M. S.; Merrill, G. N. *J. Chem. Phys.* **2000**, *112*, 2063−2073.
(23) Netzloff, H. M.; Gordon, M. S. *J. Chem. Phys.* **2004**, *121*, 2711−2714.
(24) Kemp, D. D.; Gordon, M. S. *J. Phys. Chem. A* **2008**, *112*, 4885−4894.
(25) Chen, W.; Gordon, M. S. *J. Chem. Phys.* **1996**, *105*, 11081−11090.
(26) Webb, S. P.; Gordon, M. S. *J. Phys. Chem. A* **1999**, *103*, 1265−1273.
(27) Krauss, M. *Comput. Chem.* **1994**, *19*, 33−38.
(28) Krauss, M.; Webb, S. P. *J. Chem. Phys.* **1997**, *107*, 5771−5775.
(29) Krauss, M.; Wladowski, B. D. *Int. J. Quantum Chem.* **1998**, *69*, 11−19.
(30) Minikis, R. M.; Kairys, V.; Jensen, J. H. *J. Phys. Chem. A* **2001**, *105*, 3829−3837.
(31) Arora, P.; Slipchenko, L. V.; Webb, S. P.; DeFusco, A.; Gordon, M. S. *J. Phys. Chem. A* **2010**, *114*, 6742−6750.
(32) Slipchenko, L. V. *J. Phys. Chem. A* **2010**, *114*, 8824−8830.
(33) Kosenkov, D.; Slipchenko, L. V. *J. Phys. Chem. A* **2011**, *115*, 392−401.
(34) Yoo, S.; Zahariev, F.; Sok, S.; Gordon, M. S. *J. Chem. Phys.* **2008**, *129*, 144112−1−144112−8.
(35) Minezawa, N.; Silva, N. D.; Zahariev, F.; Gordon, M. S. *J. Chem. Phys.* **2011**, *134*, 054111−1−054111−12.
(36) Benjamin, I. *Chem. Phys. Lett.* **1998**, *287*, 480−486.
(37) Sinha, H. K.; Yates, K. *Can. J. Chem.* **1991**, *69*, 550−557.
(38) Sinha, H. K.; Yates, K. *J. Am. Chem. Soc.* **1991**, *113*, 6062−6067.
(39) Farztdinov, V. M.; Schanz, R.; Kovalenko, S. A.; Ernsting, N. P. *J. Phys. Chem. A* **2000**, *104*, 11486−11496.
(40) Sim, F.; Chin, S.; Dupuis, M.; Rice, J. E. *J. Phys. Chem.* **1993**, *97*, 1158−1163.
(41) Scalmani, G.; Frisch, M. J.; Mennucci, B.; Tomasi, J.; Cammi, R.; Barone, V. *J. Chem. Phys.* **2006**, *124*, 094107−1−094107−15.
(42) Das, G. P.; Dudis, D. S. *J. Phys. Chem. A* **2000**, *104*, 4767−4771.
(43) Moran, A. M.; Kelley, A. M.; Tretiak, S. *Chem. Phys. Lett.* **2003**, *367*, 293−307.
(44) Cammi, R.; Frediani, L.; Mennucci, B.; Ruud, K. *J. Chem. Phys.* **2003**, *119*, 5818−5827.
(45) Rashid, A. N. *J. Mol. Struct.* **2004**, *681*, 57−63.
(46) Wang, C.-K.; Wang, Y.-H. *J. Chem. Phys.* **2005**, *119*, 4409−4412.
(47) Moran, A. M.; Kelley, A. M. *J. Chem. Phys.* **2001**, *115*, 912−924.
(48) Millefiori, S.; Favini, G.; Millefiori, A.; Grasso, D. *Spectrochim. Acta* **1977**, *33A*, 21−27.
(49) Thomsen, C. L.; Thøgersen, J.; Keiding, S. R. *J. Phys. Chem. A* **1998**, *102*, 1062−1067.
(50) Kovalenko, S. A.; Schanz, R.; Farztdinov, V. M.; Hennig, H.; Ernsting, N. P. *Chem. Phys. Lett.* **2000**, *323*, 312−322.
(51) Trueblood, K. N.; Goldfish, E.; Donohue, J. *Acta Crystallogr.* **1961**, *14*, 1009−1017.
(52) Breitung, E. M.; Vaughan, W. E.; McMahon, R. J. *Rev. Sci. Instrum.* **2000**, *71*, 224−227.
(53) Arnett, E. M.; Hufford, D.; McKelvey, D. R. *J. Am. Chem. Soc.* **1966**, *88*, 3142−3143.
(54) Kaatz, P.; Shelton, D. P. *J. Chem. Phys.* **1996**, *105*, 3918−3929.
(55) Runge, E.; Gross, E. K. U. *Phys. Rev. Lett.* **1984**, *52*, 997−1000.
(56) Gross, E. K. U.; Kohn, W. *Adv. Quantum Chem.* **1990**, *21*, 255−291.
(57) van Leeuwen, R. *Int. J. Mod. Phys. B* **2001**, *15*, 1969−2023.
(58) Casida, M. E., Time-dependent density-functional response theory for molecules. In *Recent Advances in Density Functional Methods*; Chong, D. P., Eds.; Recent Advances in Computational Chemistry; World Scientific: Singapore, 1995; Vol. 1, pp 155−192.
(59) Casida, M. E., Time-Dependent Density Functional Response Theory of Molecular Systems: Theory, Computational Methods, and Functionals. In *Recent Developments and Applications of Modern Density Functional Theory, Theoretical and Computational Chemistry*; Seminario, J. M., Eds.; Elsevier: Amsterdam, 1996; pp 391−439.
(60) Hirata, S.; Head-Gordon, M. *Chem. Phys. Lett.* **1999**, *314*, 291−299.
(61) Martyna, G. J.; Tuckerman, M. E.; Tobias, D. J.; Klein, M. L. *Mol. Phys.* **1996**, *87*, 1117−1157.
(62) Becke, A. D. *J. Chem. Phys.* **1993**, *98*, 5648−5652.
(63) Lee, C.; Yang, W.; Parr, G. R. *Phys. Rev. B* **1988**, *37*, 785−789.
(64) Stephens, P. J.; Devlin, F. J.; Chadalowski, C. F.; Frisch, M. J. *J. Phys. Chem.* **1994**, *98*, 11623−11627.

(65) Dunning, T. H. Jr.; Hay, P. J. Gaussian Basis Sets for Molecular Calculations. In *Methods of Electronic Structure Theory*; Schaefer, H. F., III, Eds.; Plenum: New York, 1977; Vol. 3, pp 1−27.
(66) Perdew, J. P.; Burke, K.; Ernzerhof, M. *Phys. Rev. Lett.* **1996**, *77*, 3865−3868.
(67) Adamo, C.; Barone, V. *J. Chem. Phys.* **1999**, *110*, 6158−6170.
(68) Yanai, T.; Tew, D. P.; Handy, N. C. *Chem. Phys. Lett.* **2004**, *393*, 51−57.
(69) Murray, C. W.; Handy, N. C.; Laming, G. J. *Mol. Phys.* **1993**, *78*, 997−101.
(70) Lebedev, V. I.; Laikov, D. N. *Dokl. Math.* **1999**, *59*, 477−481.
(71) Peach, M. J. G.; Benfield, P.; Helgaker, T.; Tozer, D. J. *J. Chem. Phys.* **2008**, *128*, 044118−1−044118−8.
(72) Peach, M. J. G.; Sueur, C. R. L.; Ruud, K.; Guillaume, M.; Tozer, D. J. *Phys. Chem. Chem. Phys.* **2009**, *11*, 4465−4470.
(73) Peach, M. J. G.; Tozer, D. J. *J. Mol. Struct.: THEOCHEM* **2009**, *914*, 110−114.
(74) Wiggins, P.; Williams, J. A. G.; Tozer, D, J. *J. Chem. Phys.* **2009**, *131*, 091101−1−091101−4.
(75) Dwyer, A. D.; Tozer, D. J. *Phys. Chem. Chem. Phys.* **2010**, *12*, 2816−2818.
(76) Plötner, J.; Tozer, D. J.; Dreuw, A. *J. Chem. Theory Comput* **2010**, *6*, 2315−2324.
(77) Spackman, M. A. *J. Comput. Chem.* **1996**, *17*, 1−18.
(78) Gordon, M. S.; Schmidt, M. W. Advances in Electronic Structure Theory: GAMESS: A Decade Later. In *Theory and Applications of Computational Chemistry: The First Forty Years*; Dykstra, C. E., Frenking, G., Kim, K. S., Scuseria, G. E., Eds.; Elsevier: Amsterdam, 2005; pp 1167−1189.
(79) Bode, B. M.; Gordon, M. S. *J. Mol. Graphics Modell.* **1998**, *16*, 133−138.
(80) Dreuw, A.; Weisman, J. L.; Head-Gordon, M. *J. Chem. Phys.* **2003**, *119*, 2943−2946.
(81) Zhao, Y.; Truhlar, D. G. *J. Phys. Chem. A* **2006**, *110*, 13126−13130.
(82) Autschbach, J. *Chem. Phys. Chem.* **2009**, *10*, 1757−1760.
(83) Defusco, A.; Ivanic, J.; Schmidt, M. W.; Gordon, M. S. *J. Phys. Chem. A* **2011**, *115*, 4574−4582.
(84) Bandyopadhyay, P.; Gordon, M. S.; Mennucci, B.; Tomasi, J. *J. Chem. Phys.* **2002**, *116*, 5023−5032.
(85) Aidas, K.; Møgelhøj, A.; Nilsson, E. J. L.; Johnson, M. S.; Mikkelsen, K. V.; Christiansen, O.; Söderhjelm, P.; Kongsted., J. *J. Chem. Phys.* **2008**, *128*, 194503−1−194503−15.